# An efficient simulator for pinhole imaging of PET isotopes



2011 Phys. Med. Biol. 56 1617

(http://iopscience.iop.org/0031-9155/56/6/007)

IOP PUBLISHING PHYSICS IN MEDICINE AND BIOLOGY

Phys. Med. Biol. **56** (2011) 1617–1634 doi:10.1088/0031-9155/56/6/007

# An efficient simulator for pinhole imaging of PET isotopes

**M C Goorden[1,2], F van der Have[1,3], R Kreuger[1] and F J Beekman[1,3]**

[1] Section of Radiation Detection and Medical Imaging, Applied Sciences, Delft University of Technology, Mekelweg 15, 2629 JB Delft, The Netherlands
[2] Department of Nuclear Medicine, Image Sciences Institute, University Medical Center Utrecht, Universiteitsweg 100, 3584 CG Utrecht, The Netherlands
[3] Molecular Imaging Labs (MILabs), Heidelberglaan 100, 3584 CX Utrecht, The Netherlands

E-mail: m.c.goorden@tudelft.nl

Received 28 September 2010, in final form 10 December 2010
Published 18 February 2011
Online at stacks.iop.org/PMB/56/1617

**Abstract**

Today, small-animal multi-pinhole single photon emission computed tomography (SPECT) can reach sub-half-millimeter image resolution. Recently we have shown that dedicated multi-pinhole collimators can also image PET tracers at sub-mm level. Simulations play a vital role in the design and optimization of such collimators. Here we propose and validate an efficient simulator that models the whole imaging chain from emitted positron to detector signal. This analytical simulator for pinhole positron emission computed tomography (ASPECT) combines analytical models for pinhole and detector response with Monte Carlo (MC)-generated kernels for positron range. Accuracy of ASPECT was validated by means of a MC simulator (MCS) that uses a kernel-based step for detector response with an angle-dependent detector kernel based on experiments. Digital phantom simulations with ASPECT and MCS converge to almost identical images. However, ASPECT converges to an equal image noise level three to four orders of magnitude faster than MCS. We conclude that ASPECT could serve as a practical tool in collimator design and iterative image reconstruction for novel multi-pinhole PET.

## 1. Introduction

Accurate simulation of a single photon emisssion computed tomography (SPECT) system is often a good alternative to phantom experiments and often the only way to mimic SPECT imaging of a complex activity distribution (Zubal and Harrell 1991, Zaidi 1999, Assié *et al* 2004, Staelens and Buvat 2009). A SPECT simulator can be useful in system design (Schramm *et al* 2003, Meng *et al* 2003, Beekman and Vastenhouw 2004, Cao *et al* 2005, Funk *et al* 2006, Vunckx *et al* 2009, Shokouhi *et al* 2009) and it can be applied in model-based iterative reconstruction methods (Floyd *et al* 1986, Beekman *et al* 1996, Kadrmas *et al*

  

1998, Beekman *et al* 2002, Frey *et al* 2002, Narayanan *et al* 2003, Farncombe *et al* 2004, He *et al* 2005, Moore *et al* 2006, Cot *et al* 2005, Du *et al* 2006, Xiao *et al* 2006, 2007). The main challenge that is faced in developing a simulator is to have a good balance between accuracy, variance and efficiency. A large variety of SPECT simulators have been proposed, based on analytical models, Monte Carlo (MC) simulations or a combination of these (Beck *et al* 1982, Wang *et al* 1992, Frey and Tsui 1994, Walrand *et al* 1994, Meikle *et al* 1994, Beekman and Viergever 1995, Beekman *et al* 1999, de Jong *et al* 2001, Du *et al* 2002, Gieles *et al* 2002, De Wit *et al* 2006, Staelens *et al* 2007, de Beenhouwer *et al* 2008, Liu *et al* 2008, Descourt *et al* 2010).

Fast SPECT simulators are extremely useful to (i) quickly simulate complete animal or patient SPECT studies in order to optimize acquisition, reconstruction and image processing protocols, (ii) serve as a projector in image reconstruction (e.g. in dual matrix reconstruction (Kamphuis *et al* 1997)) or (iii) generate entire system matrices as required in some image reconstruction schemes. For all these applications it is required that the simulator rapidly generates almost noiseless projections of activity distributions. Even when the influence of noise is considered (e.g. when evaluating complete SPECT systems for realistic imaging times and activity concentrations), Poisson noise is usually added to the smooth projection data, instead of using time-consuming full MC simulations (often referred to as analog MC) to generate noisy data.

Recently the use of highly focusing multi-pinhole collimators in small-animal SPECT has resulted in sub-half-millimeter image resolutions (Beekman *et al* 2005, Beekman and van der Have 2007a, Van der Have *et al* 2009). In many cases these high-resolution SPECT systems are capable of imaging even smaller structures than dedicated small-animal positron emission tomography (PET) devices; high-end PET usually has approximately 1 mm image resolution (although new ideas to obtain sub-mm resolution have been put forward, e.g. Tai *et al* 2008). This naturally raises the question if positron emitters can be imaged at high resolutions using a dedicated multi-pinhole geometry (Beekman and van der Have 2007b).

In Beekman (2008) clustered multi-pinhole PET was proposed, a new technology that enables high-resolution imaging of positron emitting tracers (Goorden and Beekman 2010a). The potential of clustered multi-pinhole PET was confirmed by recent experiments, which report simultaneous SPECT-PET imaging at sub-mm resolutions (Beekman *et al* 2010, Goorden *et al* 2010b). Pinhole PET is still in an early stage of development and it is an open question in which subset of imaging situations pinhole PET is able to compete with coincidence PET. Pinhole PET has the added advantage that it provides perfectly aligned PET and SPECT images and it may save costs and floor space because only a single device needs to be purchased for SPECT and PET imaging.

For further development of multi-pinhole PET collimators, optimization of pinhole PET imaging protocols and for the generation of realistic system matrices for image reconstruction, an accurate and efficient simulator of these systems is highly desirable. In this paper we present an analytical simulator for pinhole positron emission computed tomography (ASPECT) which takes into account (i) the finite positron range, (ii) collimator blurring and (iii) detector response. We evaluate the accuracy and speed-up attained by ASPECT by comparing it with a MC simulator (MCS).

## 2. Methods

This section starts with a description of the implementation of ASPECT. Next, MCS that is used to validate ASPECT is discussed. Finally we comment on computer simulations used to determine the accuracy and speed-up of ASPECT with respect to MCS.

### 2.1. Implementation of ASPECT

ASPECT consists of three parts. Initially the activity distribution is blurred by a probability distribution $P_\beta$, which describes the effects of finite positron range; it is based on a look-up table that is generated by MC simulations. Subsequently, pinhole response is simulated using an analytical pinhole model. Finally, the detector response is approximated by a Gaussian kernel with fixed full width at half maximum (FWHM) that is independent of angle of incidence. Details for positron range simulations and pinhole response are provided below.

*2.1.1. MC simulations for positron range.* The MC software used in this paper is Geant4 version 9.1. Geant is an acronym for 'geometry and tracking' and it provides a toolkit for the simulation of particles through matter. The program has been developed by CERN and its collaborators (CERN[4], Agostinelli *et al* 2003), and has been extensively validated for the simulation of PET and SPECT (Staelens *et al* 2003, 2006, Strul *et al* 2003, Santin *et al* 2003, Jan *et al* 2004). For the simulations in this work the low-energy extensions for the photoelectric effect, the Compton effect, Rayleigh scattering, ionization and bremsstrahlung were used.

The effects of positron range are captured by the annihilation point distribution function $P_\beta(x, y, z)$, a spherically symmetric distribution that describes the displacement of the annihilation site from the point of positron emission. The positron range and its effects on system resolution have been studied in the past using experiments and MC simulations (Derenzo 1979, Derenzo 1986, Levin and Hoffman 1999). In these previous works, however, only projections of the three-dimensional distribution have been presented and we can therefore not incorporate the results of these papers directly into our simulator. To obtain the full three-dimensional distribution, we have performed MC simulations of the trajectories of positrons in water. The energy of the positron is generated using the analytical expression for the energy spectrum $N(E)$, given by

$$N(E) = gF(Z, E)pE(E_{\max} - E)^2. \tag{1}$$

Here $g$ is a coupling constant, $F(Z, E)$ is the Fermi function, $Z$ is the atomic number of the beta decay daughter and $p$ is the momentum. In this paper we consider $^{18}$F, which has a maximum (end point) energy $E_{\max} = 635$ keV.

We have simulated 5 million positron decays all occurring at the same location and the end points of the positron trajectories were stored. Assuming that the location of positron decay was in the center of a voxel, we generated a look-up table that contains the probability that a positron that is emitted in one voxel annihilates in another nearby voxel. Voxel size was 0.4 mm, equal to the voxel size of the simulated phantom (see section 2.4). With this look-up table the activity distribution is convolved. Note that the choice of taking the positron decay position in the center of the voxel is in agreement with the approach taken in ASPECT to simulate one photon path from each voxel to each detector pixel (see below).

In real subjects, the use of a positron range kernel that reflects an infinite source of water is an approximation. A more accurate model would take different materials and boundaries into account. However, even the use of such a simplified blurring kernel, that represents the positron range in water, can significantly improve reconstructed images in PET animal experiments (Ruangma *et al* 2006).

*2.1.2. Analytical model for pinhole response.* The geometry of a pinhole in the plane through pinhole axis and source is shown in figure 1(a). We consider a knife-edge pinhole with opening angle $\alpha$ and diameter $d$. A point source is placed at position $\boldsymbol{S}$, at a distance $h$ above the pinhole

[4] CERN GEANT4 homepage http://geant4.web.cern.ch/geant4

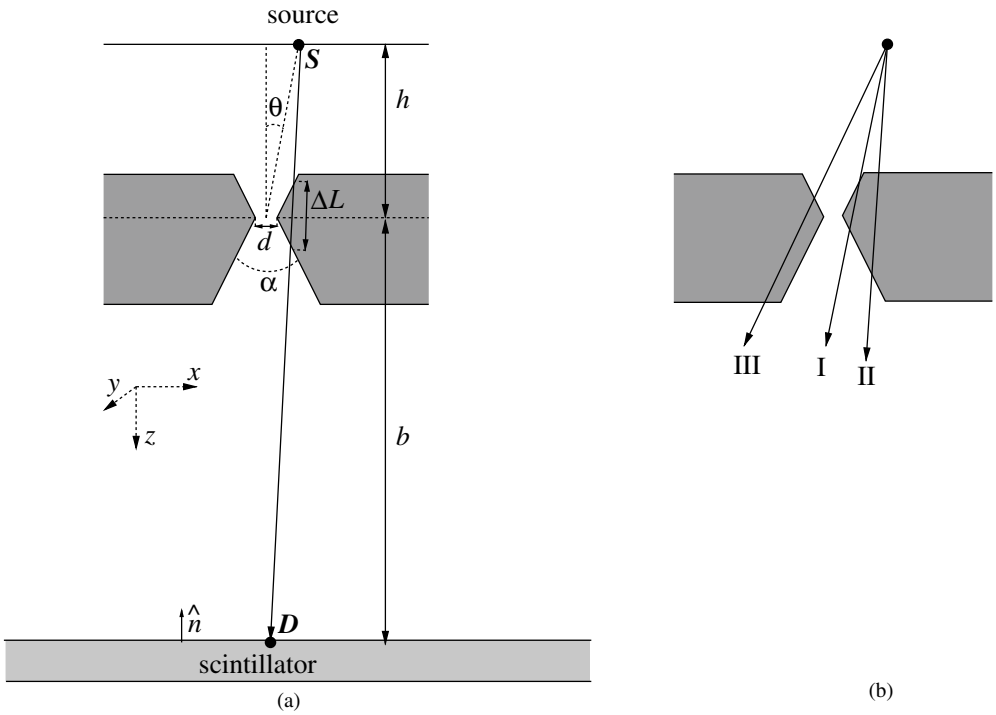


**Figure 1.** (a) Geometry of a simulated source-collimator-detector system. The photon source is positioned at an angle $\theta$ and at a distance $h$ above the pinhole aperture. The pinhole has an opening angle $\alpha$ and diameter $d$ and is placed at a distance $b$ from the detector. (b) A pinhole with three different types of photon paths; path I passes through the cone-shaped pinhole surfaces only. Paths II and III cross a cone-shaped pinhole surface and a collimator wall plane.

aperture and at an angle of incidence $\theta$. An analytical model for the point spread function (PSF) due to the pinhole aperture is obtained by taking into account photons that penetrate the pinhole edges, but ignoring photons that scatter (Metzler *et al* 2002). The application of this analytical model in pinhole SPECT simulations has already been validated for gamma photons of 140 keV (corresponding to $^{99m}$Tc) (Gieles *et al* 2002), but it has never been tested for 511 keV gamma photons.

The intensity at position $\boldsymbol{D}$ on the detector is given by

$$\mathrm{PSF}_{\mathrm{pinh}}(\mathbf{D},\mathbf{S}) = \frac{(\mathbf{S}-\mathbf{D})\cdot\hat{\mathbf{n}}}{4\pi\,|\mathbf{S}-\mathbf{D}|^3}\,\mathrm{e}^{-\mu\Delta L}. \tag{2}$$

Here $\hat{\mathbf{n}}$ is a unit vector normal to the detector surface, $\mu$ is the attenuation coefficient of the pinhole aperture material at the energy of the incident photons and $\Delta L$ is the path length through the aperture material.

An analytical expression for the path length through a pinhole is given in Gieles *et al* (2002). We use their equations, but we make one adaptation, which is necessary to accurately describe 511 keV gamma photons. This is illustrated in figure 1(b), where three types of photon paths through a pinhole are sketched. Path I passes through the cone-shaped pinhole surfaces only. Paths II and III, however, also pass through the collimator wall. The expressions in Gieles *et al* (2002) do not consider this possibility and they are only strictly valid for infinitely

long pinholes. While for 140 keV the pinholes are sufficiently long for this to be a good approximation, it cannot be safely assumed that this also holds for the 511 keV annihilation photons considered in this paper. We do therefore explicitly take the possibility of penetrating the collimator wall into account.

We consider one photon path from the center of each voxel (containing annihilations) to each relevant detector pixel. Relevant detector pixels are determined by directing the photons only to a circular area in the pinhole aperture (Gieles *et al* 2002), such that all photons with a probability as low as $10^{-3}$ to be transmitted through the collimator material are taken into account.

### *2.2. Implementation of MCS*

The MCS that is used to validate ASPECT uses the Geant4 MC software package (version 9.1) to simulate the events from positron decay up to a photon entering the gamma detector. In the simulations the energy window at the detector is set to an interval of 461–561 keV. The detector response is very sensitive to various optical parameters of the scintillator and to the specific implementation of the electronics and it is therefore difficult to simulate this response accurately. For this reason we have incorporated detector blurring using a kernel-based approach based on the experimentally obtained angle-dependent detector response (measurements were done for four angles of incidence, see below). Bi-cubic interpolation is used to obtain the detector response for a gamma photon entering the detector at an arbitrary angle. The detector experiments performed to obtain this kernel are described below.

*2.2.1. Detector response experiments.* USPECT-II has three scintillation gamma camera heads with sodium iodide (NaI) crystals having a thickness of 3/8 inch (9.5 mm) and a useful detection area of 490 × 400 mm. Each crystal is read out by 55 photomultiplier tubes (PMTs). To determine the detector response of such a gamma detector to 511 keV gamma photons and compare it with the known response to 140 keV photons from $^{99m}$Tc we have constructed a collimating piece of lead that restricts the gamma photons to four pencil beams incident at different angles onto the detector (see figure 2). It consists of a 47 mm thick piece of lead with four $1 \times 1$ mm$^2$ square channels. The four channels have angles of 90°, 80°, 70° and 60° with respect to the detector surface. A plastic source holder is positioned at the intersection point of the four channels. The source holder has a cylindrically shaped hole with a diameter of 2.2 mm in it, which can be filled with a solution of a radionuclide.

Measurements were performed for a source of $^{99m}$Tc and $^{18}$F-fludeoxyglucose (FDG). The starting activity of $^{99m}$Tc and FDG was 6.3 MBq and 4.1 MBq, respectively. The collimator was placed at five different positions on one of the three detector heads of U-SPECT-II to obtain an average detector response. The energy window was set to an interval of 461–561 keV for FDG and to 126–154 keV for $^{99m}$Tc. The results that we present in the results section are PSFs that are averaged over the five detector positions.

### *2.3. Parameters of the simulated set-up*

The simulated set-up is shown in figure 1(a). We choose parameters corresponding to the high-resolution MP-SPECT system proposed in Goorden and Beekman (2010a), that is specially designed to image PET tracers in a mouse at high resolutions. This system has a cylindrical multi-pinhole collimator. We assume that the point source is on the axis of the cylindrical collimator, which is at a distance of 28 mm from the pinhole center ($h = 28$ mm in figure 1(a)). Furthermore, the detector is at a distance of 182 mm from the pinhole center

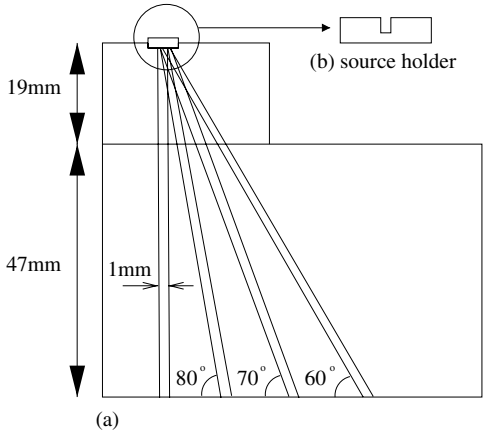


**Figure 2.** (a) Design of the collimating piece of lead; (b) shape of the plastic source holder. The cylindrical hole in the source holder can be filled with a solution of a radionuclide.

($b = 182$ mm in figure 1(a)). The pinhole is placed asymmetrically in the collimator wall which has a thickness of 45 mm. We consider pinhole opening angles of $\alpha = 30^\circ$ and $\alpha = 15^\circ$, each with a pinhole diameter $d = 0.6$ mm. The detector pixel size was 0.5 mm $\times$ 0.5 mm.

### *2.4. Validation and speed-up*

First, the accuracy of the analytical models for pinhole and detector response implemented in ASPECT were validated. To this end the analytical pinhole response (equation (1)) to a point source of 511 keV gamma photons in air was compared to MC simulations. Like in the simulations described in previous paragraphs, Geant4 version 9.1 was used. We considered three point source positions; from the center up to the edge of the pinhole field-of-view (FOV). Next, to evaluate how well the approximation of an angle-independent Gaussian detector model (implemented in ASPECT) holds for a typical pinhole response, we have blurred these simulated pinhole responses either with a FWHM 3.5 mm Gaussian kernel or with the experimentally measured angle-dependent detector kernel and we compare these.

After having considered the individual parts of ASPECT, we validated the whole simulator. We compared the projections of an extended source onto the detector obtained with ASPECT and MCS. The main reason to compare ASPECT and MCS for an extended source is to assess the amount of gamma photons that scatter in the object and at the pinhole edges. In ASPECT, scattering is ignored. Scattered photons may have a small magnitude in a PSF, but these are typically spread over a much larger detector area than the PSF itself. We determined the magnitude of the scattering contribution by presenting projections with and without scattering (scattered photons can easily be identified in MC simulations). The source that was simulated is an ellipse with radii of 5 $\times$ 3.5 $\times$ 6 mm (typical for a mouse organ such as the brain), placed in a larger water-filled ellipse that has the size of a mouse and a voxel size of 0.4 mm. We have simulated $10^{11}$ positron decays in the MCS to get an almost noise-free projection.

The simulations described above were done in order to assess the accuracy (bias) of ASPECT with respect to MCS. We subsequently determined the speed-up that can be obtained by ASPECT with respect to MCS by comparing simulation times at equal variance (noise level). To this end the almost noise-free projection obtained with MCS (see previous paragraph) is used as a reference projection. A series of projections was generated with MCS with an

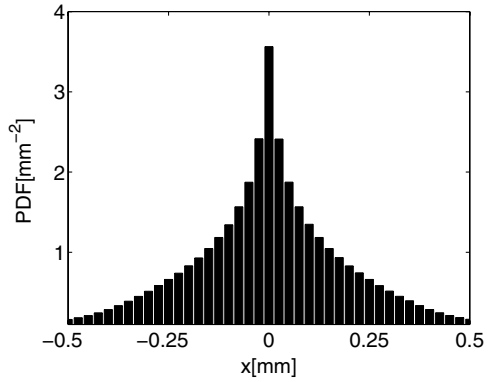


**Figure 3.** Probability density distribution (PDF) of the $x$ coordinates of the end points of the simulated positron trajectories.

increasing number of simulated positron emissions and hence, an increasing simulation time. For each of these projections the normalized mean square error (NMSE) with respect to the reference projection was determined. The NMSE that is achieved with ASPECT was also determined by comparing the projection generated by ASPECT to the reference projection, with the omission of scattered photons. This is done because we are interested in the time it takes to achieve a smooth projection and not in the bias that is inevitably present because of the neglect of scattered photons. The speed-up factor achieved by ASPECT with respect to MCS is determined by comparing simulation times at equal NMSE.

## 3. Results

### *3.1. Positron range*

In figure 3 we show a histogram of $x$ coordinates of the positron trajectory end point. Using the three-dimensional end points of 5 million positron trajectories, all starting at the same initial point, we have generated a look-up table, which contains the probability that a positron that is emitted in a particular voxel will annihilate in a certain other voxel. The distribution shown in figure 3 has a FWHM of 0.10 mm and a root mean square value of 0.33 mm. This is in excellent agreement with results reported in the literature (Levin and Hoffman 1999).

### *3.2. Pinhole response*

The validation of the analytical pinhole response model by MC simulations is shown in figure 4 for pinhole opening angle $\alpha = 30^\circ$ and for point sources incident at three different angles: from the center of the FOV ($\theta = 0^\circ$, see figure 1(a)) up to the border of the FOV ($\theta = 15^\circ$). We show PSF profiles along $x$- and $y$-directions on the detector (defined in figure 1(a)). In figure 5 similar results for $\alpha = 15^\circ$ are shown. In all cases, the MC simulation results cannot be visually distinguished from those of the analytical pinhole model.

### *3.3. Detector experiments*

Figure 6 shows the measured detector response to 511 keV and 140 keV gamma photons incident at angles of 90°, 80°, 70° and 60° with respect to the detector plane. To allow

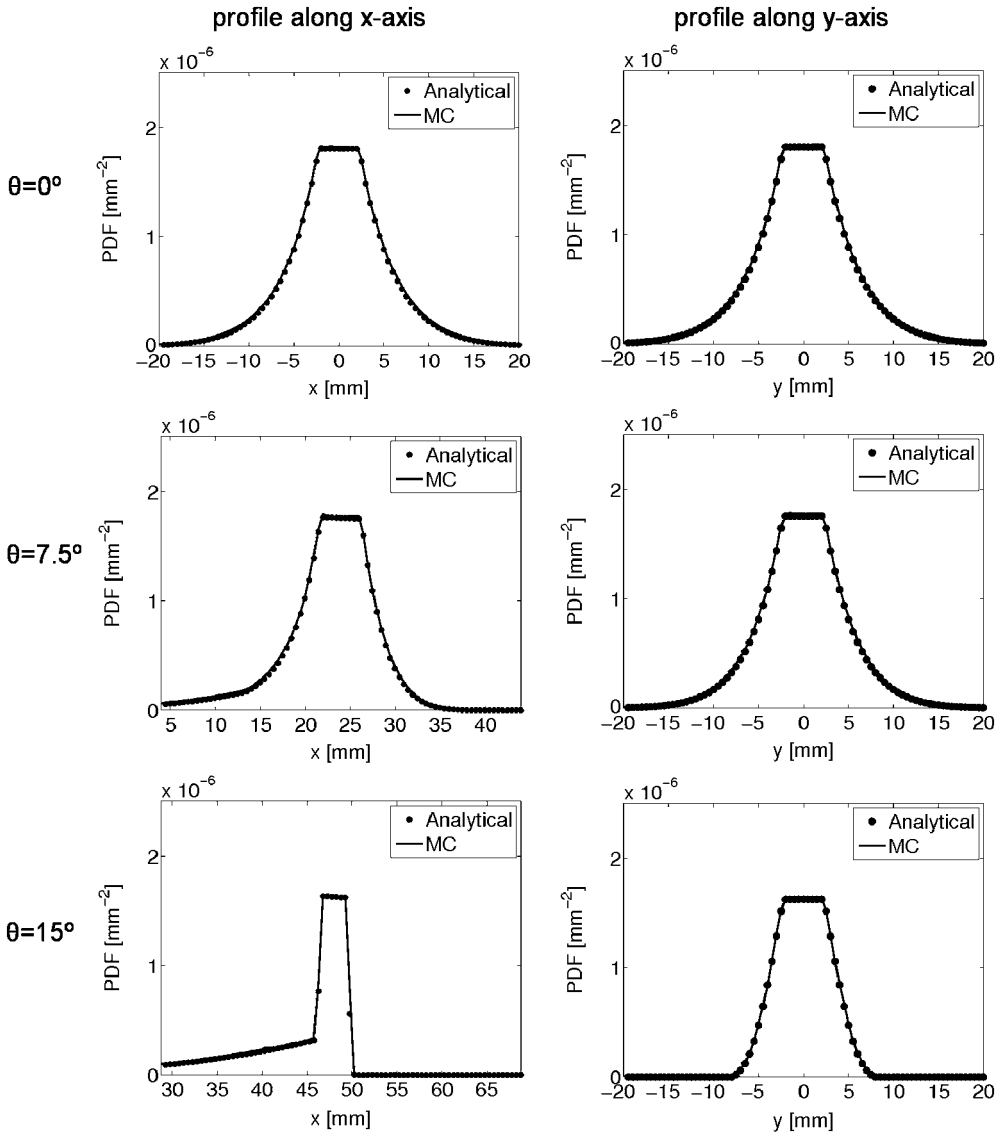


**Figure 4.** Comparison between the analytical pinhole response model and MC simulations for a point source of 511 keV in air for angles of incidence $\theta = 0^\circ$, $7.5^\circ$ and $15^\circ$. Profiles along $x$- and $y$-directions (see figure 1) are shown. For all plots $h = 28$ mm, $b = 182$ mm and $\alpha = 30^\circ$.

for a visual comparison, we have scaled both PSFs to contain an equal number of counts. The FWHM of the detector response as a function of the angle of incidence is shown in figure 7. For perpendicular incidence, the FWHM for 511 keV gamma photons is slightly better than that for 140 keV gamma photons. For incidence under an angle, the detector intrinsic resolution for 511 keV gamma photons degrades faster than for 140 keV gamma photons.

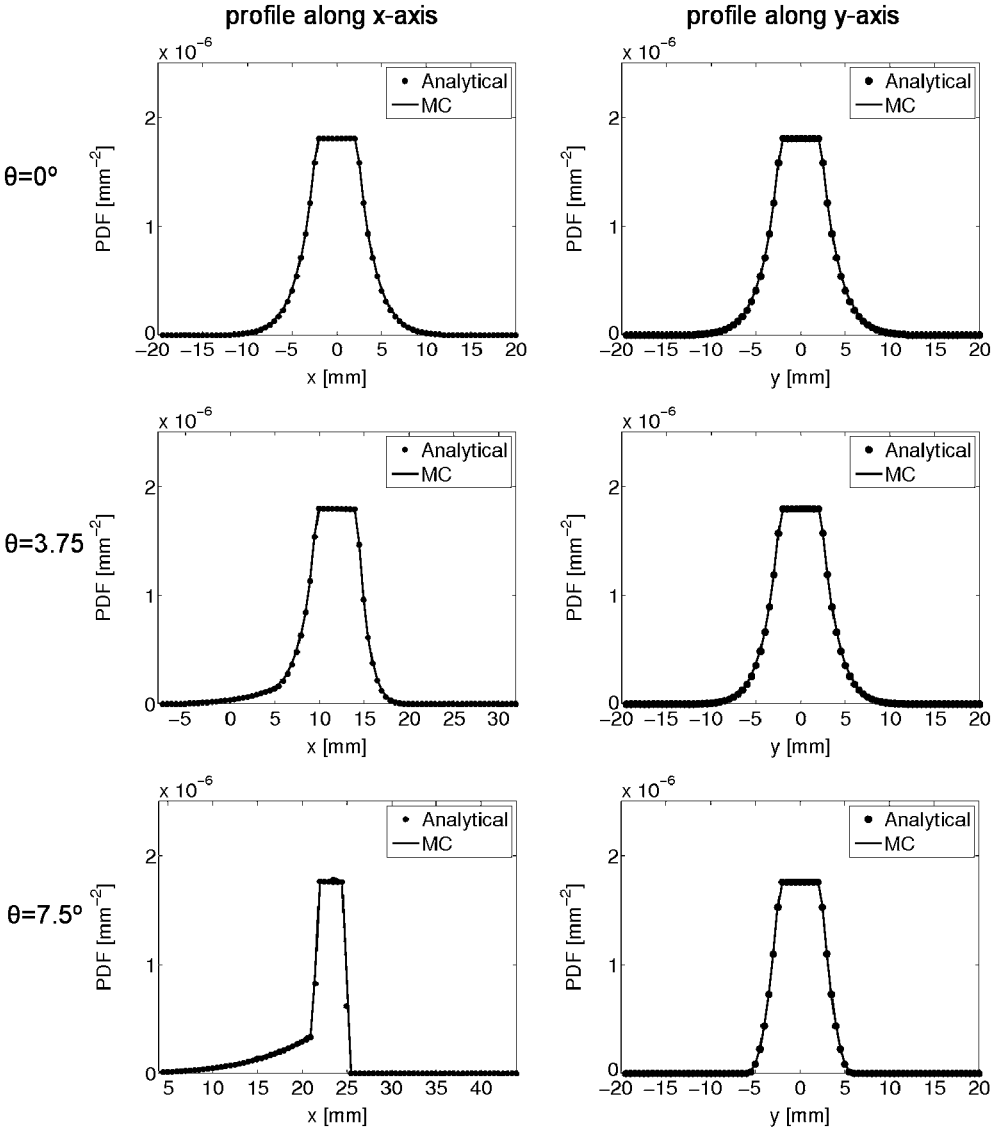


**Figure 5.** Comparison between the analytical pinhole response model and MC simulations for a point source of 511 keV in air for angles of incidence $\theta = 0^\circ$, $3.75^\circ$ and $7.5^\circ$. Profiles along $x$- and $y$-directions (see figure 1) are shown. For all plots $h = 28$ mm, $b = 182$ mm and $\alpha = 15^\circ$.

Different effects can affect intrinsic detector resolution. On one hand, 511 keV gamma photons generate more optical photons per scintillation event than gammas from $^{99m}$Tc, which allows for a better position estimation because of improved statistics. On the other hand, the depth of interaction (DOI) of a 511 keV gamma photon has a much larger spread than for 140 keV gamma photons which mainly interact in the top of the scintillator. Such a variable DOI has a detrimental effect on resolution for gamma photons entering the scintillator at an angle. Furthermore the increased chance of having multiple Compton interactions for 511 keV compared to 140 keV can also deteriorate detector resolution.

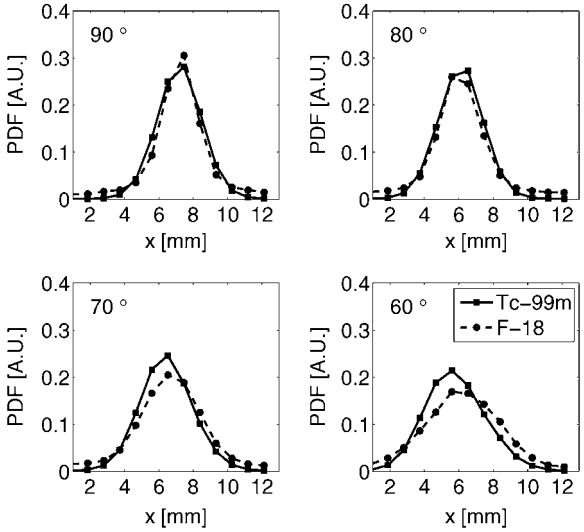


**Figure 6.** Measured probability density functions (PDFs) for beams incident at angles of 90°, 80°, 70° and 60° onto the detector surface for $^{18}$F and $^{99m}$Tc.

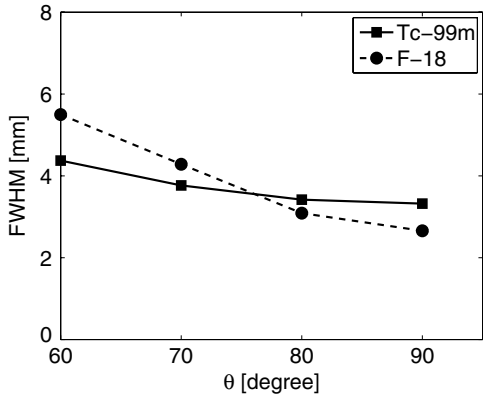


**Figure 7.** FWHM of the detector response as a function of the angle of incidence $\theta$.

Our experimental results imply that for perpendicular incidence, the increased number of optical photons that are generated for a 511 keV gamma photon compared to a 140 keV gamma photon outweighs the adverse effects of multiple Compton interactions and variable DOI and therefore resolution was slightly improved. For incidence at an angle, the effect of the variable DOI becomes more important. We therefore believe that the fast degradation of intrinsic resolution for oblique incidence of 511 keV gamma photons is mainly due to this effect.

In ASPECT we have approximated the detector response by a Gaussian kernel with a constant FWHM. From figures 6 and 7, it may seem that this is a very crude approximation. However, the accuracy of this assumption for the overall system PSF does not depend on how well the measured response approximates a Gaussian, but on how this assumption affects

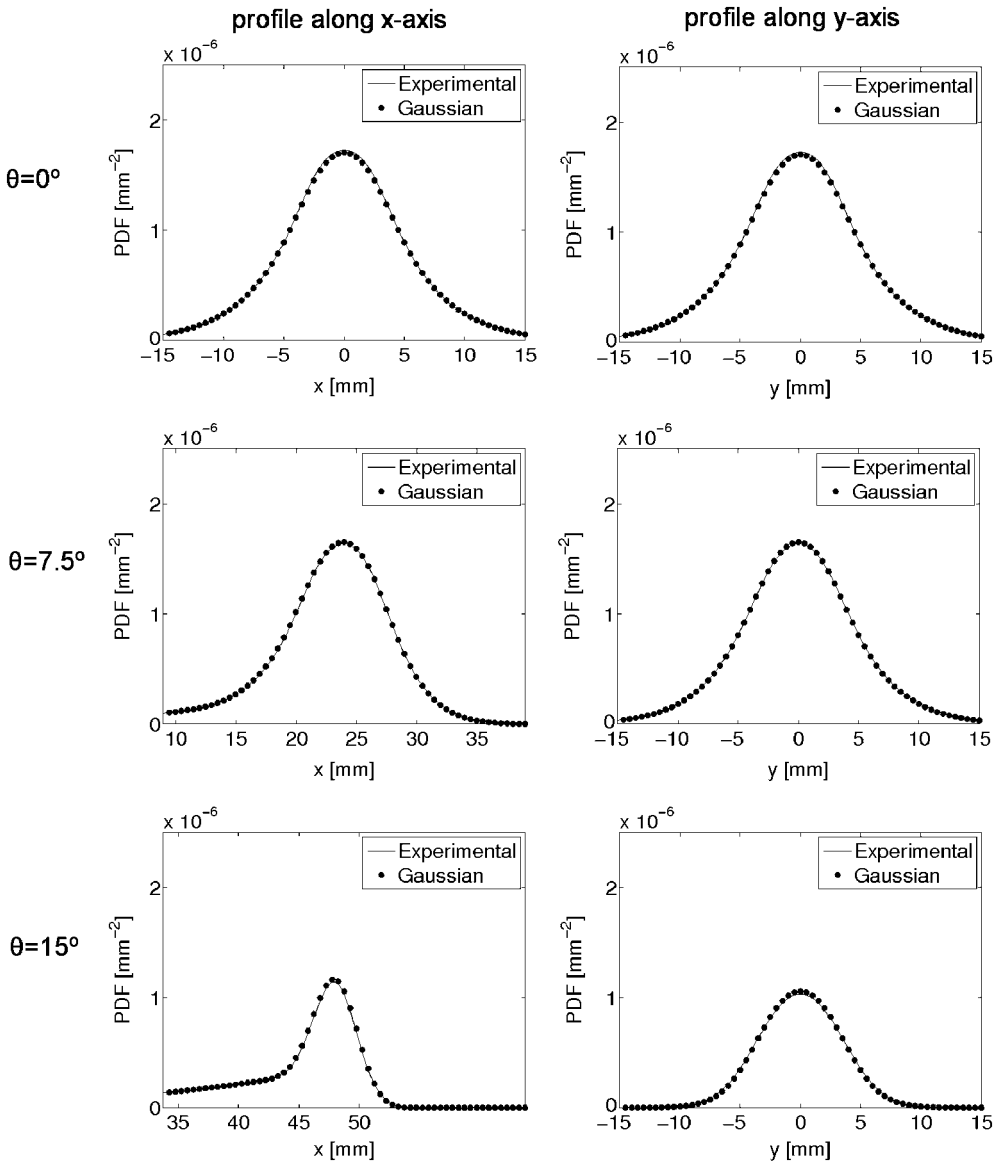


**Figure 8.** Pinhole responses of figure 5 (pinhole opening angle $\alpha = 30^\circ$) blurred with the measured 511 keV detector response (solid line) and with a Gaussian with FWHM of 3.5 mm (dots); this plot shows that a Gaussian response is a good model for detector blurring.

the shape of the overall PSF. Therefore, in figures 8 and 9 we show how the approximation of a Gaussian detector kernel affects the overall collimator response by blurring the pinhole responses of figures 4 and 5 either by the experimentally measured response or a Gaussian with a FWHM of 3.5 mm (as is implemented in ASPECT). The differences are very small and the assumption of a Gaussian response with a FWHM of 3.5 mm is expected to give a good description of detector influence. The value of 3.5 mm was chosen because it represents an average over different angles of incidence. Since a Gaussian response with this value gives a

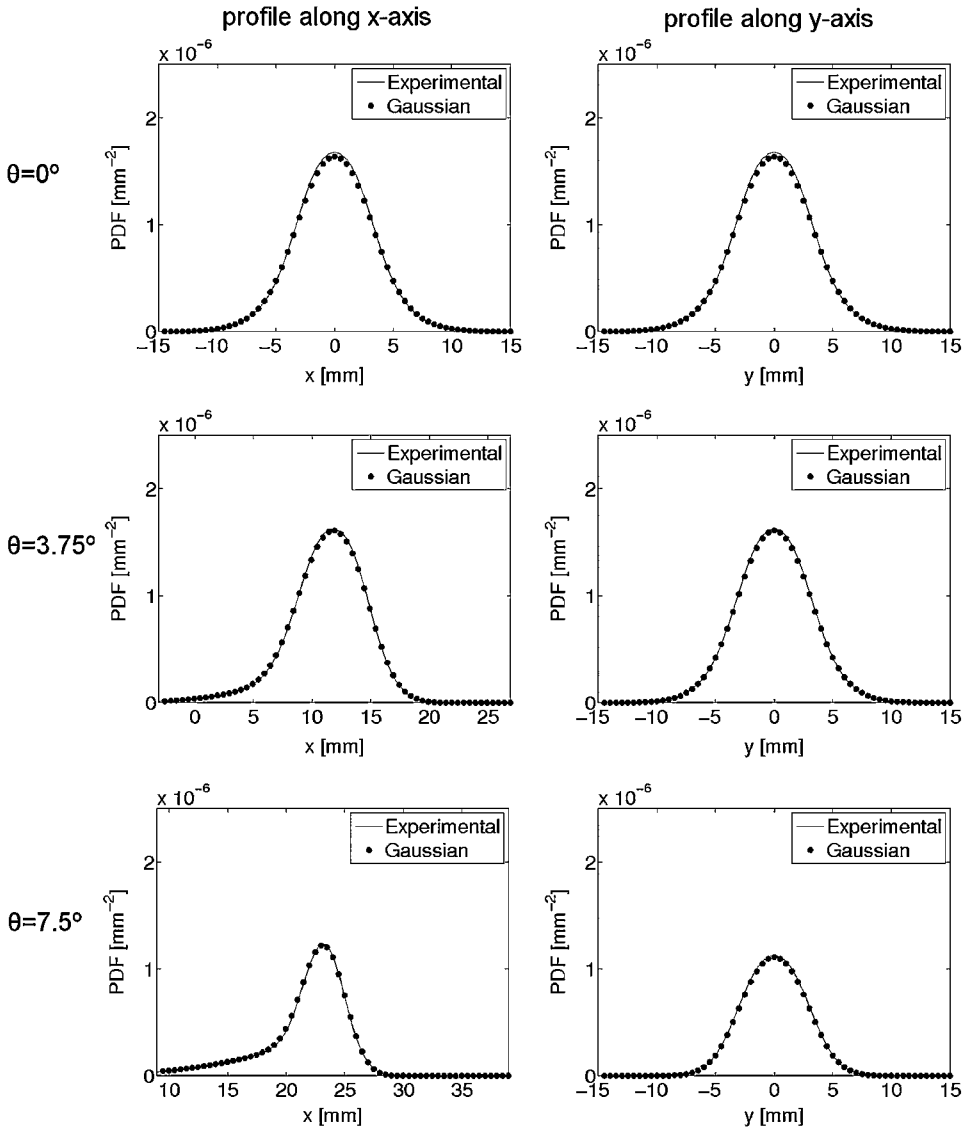


**Figure 9.** Pinhole responses of figure 6 (pinhole opening angle $\alpha = 15^\circ$) blurred with the measured 511 keV detector response (solid line) and with a Gaussian with FWHM of 3.5 mm (dots); this plot shows that a Gaussian response is a good model for detector blurring.

good description of detector blurring for all angles of incidence we believe that the results are not very sensitive to the exact FWHM that one chooses.

### *3.4. Simulation of an extended source*

In figure 10 we show the projection of the extended activity distribution onto the detector using ASPECT and MCS for pinhole opening angles $\alpha = 30^\circ$ and $\alpha = 15^\circ$. We also show the results obtained with MCS without the contribution of scattered photons. It is clear that the

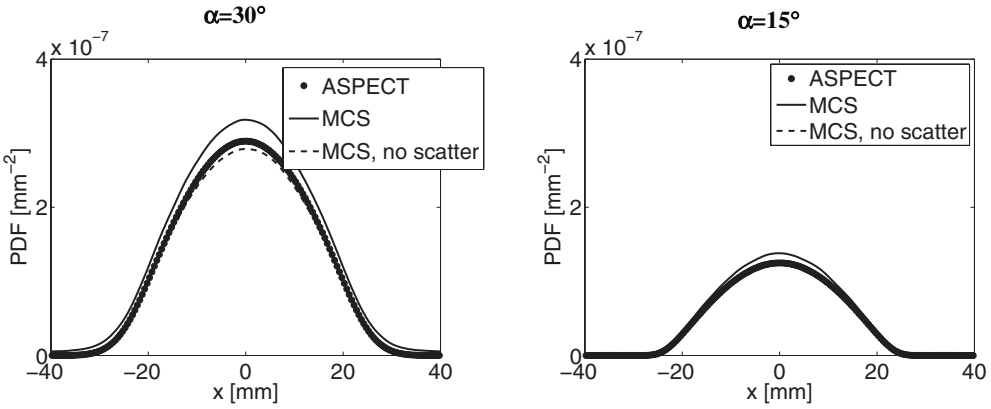


**Figure 10.** Projections of the extended activity distribution onto the detector with ASPECT (dots), MCS (solid line) and MCS without scattered photons (dotted line), for pinhole opening angles $\alpha = 30^\circ$ and $\alpha = 15^\circ$.

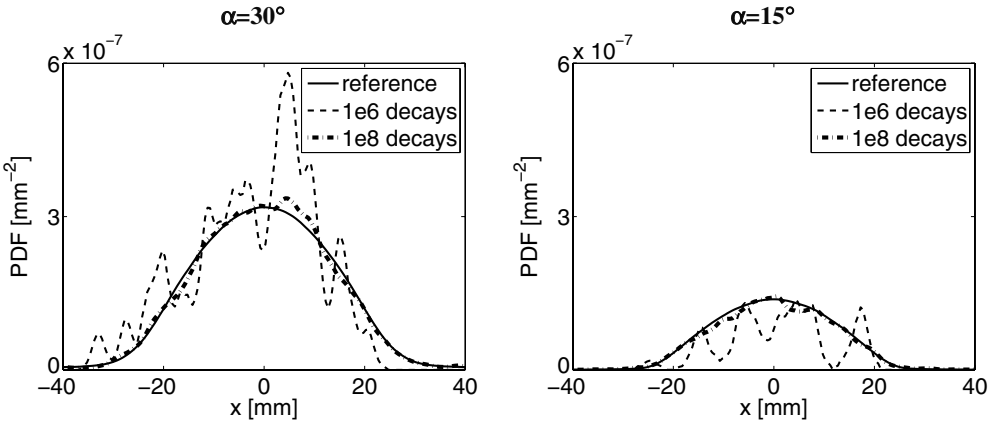


**Figure 11.** Reference projection of the extended activity distribution onto the detector together with two MCS projections with limited statistics due to a limited number of simulated positron emissions, for pinhole opening angles $\alpha = 30^\circ$ and $\alpha = 15^\circ$.

scattered photons have a small but visible effect on the simulated projection; we find that the density of scattered photons has a maximum value of $2.4\times10^{-8}$ mm$^{-2}$ and $9.2\times10^{-9}$ mm$^{-2}$ for $\alpha = 30^\circ$ and $\alpha = 15^\circ$, respectively. These numbers amount to 7.6% and 6.7% of the total maximum density.

### *3.5. SPEED-UP*

With ASPECT it takes 139 s (for $\alpha = 30^\circ$) and 63 s (for $\alpha = 15^\circ$) to simulate the projection depicted in figure 10. Compared to the reference projection (without scattered photons), an NMSE of $7.6\times10^{-9}$ and $8.7\times10^{-9}$ is found for $\alpha = 30^\circ$ and $\alpha = 15^\circ$ respectively.

Figure 11 illustrates how the number of simulated positron emissions in MCS influences the projection, by showing the noiseless reference projection together with two projections

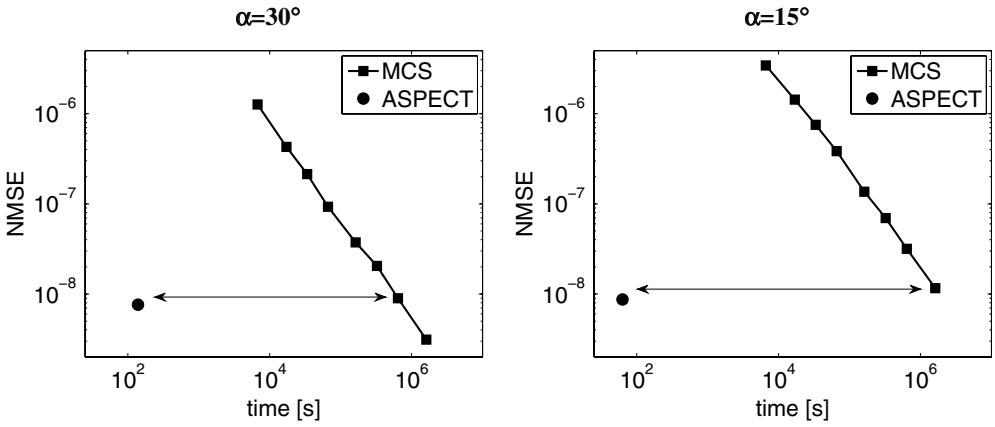


**Figure 12.** NMSE versus simulation time for a number of MCS projections and for ASPECT, for pinhole opening angles $\alpha = 30^\circ$ and $\alpha = 15^\circ$. The speed-up factor of ASPECT with respect to MCS is determined by comparing simulation time at equal NMSE (indicated by the arrows).

with different numbers of simulated positron emissions. It is clear from figure 11 that a smooth projection requires the simulation of millions of emissions, making such simulations extremely time consuming. Figure 12 shows the NMSE of MCS compared to the noiseless reference projection for increasing simulation time (due to an increasing number of simulated decays). NMSE and simulation time of ASPECT are also shown in this figure. From this figure it is clear that MCS takes orders of magnitude more time to converge to an equal noise level as ASPECT; ASPECT obtains equal NMSE $6.2\times10^3$ and $2.7\times10^4$ times as fast as MCS for $\alpha = 30^\circ$ and $\alpha = 15^\circ$ respectively (numbers are obtained by linear interpolation).

## 4. Discussion

The simulator presented in this paper is three to four orders of magnitude faster than a MC-based simulator (depending on the pinhole opening angle); with ASPECT an extended distribution having the size of a mouse organ can be simulated in approximately a minute while MCS needs weeks to reach an equal noise level. This means that, contrary to MCS, ASPECT is able to simulate complete SPECT systems within an acceptable amount of time and it can therefore be used in the evaluation of novel collimator designs or serve as the basis of model-based image reconstruction of pinhole PET systems.

The enormous speed-up of ASPECT compared to MCS is achieved despite the fact that in MCS detector response is incorporated using a kernel-based approach, rather than sampling from the probability distribution for a gamma photon that enters the scintillation crystal to end up in a certain detector pixel. This means that for each simulated gamma photon that enters the detector, many detector pixels are assigned an output signal, leading to a large speed-up compared to the usual MC approach where only one detector pixel would be reached per incident gamma photon. Therefore, if a standard MC package such as Geant4 would be used to simulate the whole system, and not only the events up to a gamma photon entering the detector as is done in this paper, even larger speed-up factors would be obtained.

The main source of deviation of ASPECT with a MC-based simulator is the neglect of scattered photons, which constitutes at most 6.7% ($\alpha = 15^\circ$) and 7.6% ($\alpha = 30^\circ$) of the

maximum photon density for an extended distribution. In Goorden and Beekman (2010) we have already shown that in a mouse the typical number of detected photons coming from organs outside the CFOV is an order of magnitude higher than the amount of scattering reported here. We therefore believe that neglecting scattered photons has a small effect on simulated images.

Another approximation of ASPECT is the assumption that a single-photon path per detector pixel is sufficient to mimic photon transport through the pinhole aperture. This approximation does not have a visible effect on the accuracy of the simulated projections in this paper. For detectors with larger pixel size than the 0.5 mm considered here, it may be necessary to sample each detector pixel more than once. Since in that case fewer pixels are present we expect similar simulation times.

The simulations to validate ASPECT were done for pinhole opening angles of 30° and 15°. These pinhole opening angles are typical of high-resolution multi-pinhole SPECT collimators (e.g. van der Have *et al* 2009) and for clustered pinhole PET (Goorden and Beekman 2010a), respectively. In these multi-pinhole geometries, all pinholes focus simultaneously on the central-field-of-view (CFOV), which has approximately the size of a mouse organ (12 mm diameter). Such a focusing geometry allows an excellent sensitivity-resolution trade-off, but it does not hinder whole body mouse imaging; high-resolution whole body mouse scans can be obtained by moving the animal through the focus (Vastenhouw and Beekman 2007). In this paper we have not considered larger pinhole opening angles than 30° since such a pinhole would be unsuitable for pinhole PET due to the large amount of pinhole edge penetration.

With our experiments we have validated the use of a Gaussian detector response for a conventional gamma detector with a 9.5 mm thick NaI(Tl) scintillator. It was shown in this paper that a Gaussian function with a fixed FWHM is adequate to describe detector response at all relevant angle of incidence. Such an assumption may have to be reevaluated for detectors with lower intrinsic resolutions (e.g. a much thicker detector) or when the magnification factor of the object onto the detector is much lower (in that case detector response has a relatively stronger effect on the PSFs). Furthermore, the amount of scattering reported here was evaluated for a typical activity distribution: a uniform distribution that has the size of a mouse brain placed in a mouse-sized water-filled ellipse. Since the exact amount of scattered photons is object dependent, further simulations may be required for other activity distributions.

## 5. Conclusions

We have presented a rapid simulator for pinhole PET that is able to generate noiseless projections several orders of magnitude faster than MC simulations. Such an efficient simulator can serve as a practical tool in the design of novel multi-pinhole collimators dedicated to imaging PET tracers, for model-based iterative image reconstruction and to optimize imaging protocols.

## References

Agostinelli S *et al* 2003 GEANT4—a simulation toolkit *Nucl. Instrum. Methods Phys. Res.* A **506** 250–303

Assié K *et al* 2004 Monte Carlo simulation in PET and SPECT instrumentation using GATE *Nucl. Instrum. Methods Phys. Res.* A **527** 180–9

Beck J W, Jaszczak R J, Coleman R E, Starmer C F and Nolte L W 1982 Analysis of SPECT including scatter and attenuation using sophisticated Monte Carlo modeling methods *IEEE Trans. Nucl. Sci.* **29** 506–11

Beekman F J 2008 Collimator with pinhole clusters *European Patent* Application No 07076118.4

Beekman F J, de Jong H W A M and Slijpen E T P 1999 Efficient SPECT scatter response estimation in non-uniform media using correlated Monte Carlo simulation *Phys. Med. Biol.* **44** N183–92

Beekman F J, de Jong H W A M and van Geloven S 2002 Efficient fully 3-D iterative SPECT reconstruction with Monte Carlo-based scatter compensation *IEEE Trans. Med. Imaging* **21** 867–77

Beekman F J, Kamphuis C and Viergever M A 1996 Improved SPECT quantitation using fully three-dimensional iterative spatially variant scatter response compensation *IEEE Trans. Med. Imaging* **15** 491–99

Beekman F J and van der Have F 2007a The pinhole: gateway to ultra-high-resolution three-dimensional radionuclide imaging *Eur. J. Nucl. Med. Mol. Imaging* **34** 151–61

Beekman F J and van der Have F 2007b High resolution tomography of positron emitters using highly focused pinhole collimation *J. Nucl. Med.* **48** 92P-b

Beekman F J, van der Have F, Kreuger R and Goorden M C 2010 Simultaneous sub-millimetre PET and SPECT with a dedicated multi-pinhole geometry *WMIC* Abstract 0041

Beekman F J, van der Have F, Vastenhouw B, van der Linden A J A, van Rijk P P, Burbach J P H and Smidt M P 2005 U-SPECT-I: a novel system for submillimeter-resolution tomography with radiolabeled molecules in mice *J. Nucl. Med.* **46** 1194–200

Beekman F J and Vastenhouw B 2004 Design and simulation of a high-resolution stationary SPECT system for small animals *Phys. Med. Biol.* **49** 4579–92

Beekman F J and Viergever M A 1995 Fast SPECT simulation including object shape dependent scatter *IEEE Trans. Med. Imaging* **14** 271–82

Cao Z, Bal G, Accorsi R and Acton P D 2005 Optimal number of pinholes in multi-pinhole SPECT for mouse brain imaging—a simulation study *Phys. Med. Biol.* **50** 4609–24

Cot A, Falcon C, Crespo C, Sempau J, Pareto D, Bullich S, Lomena F, Calvino F, Pavia J and Ros D 2005 Absolute quantification in dopaminergic neurotransmission SPECT using a Monte Carlo-based scatter correction and fully 3-dimensional reconstruction *J. Nucl. Med.* **46** 1497–504

de Beenhouwer J, Staelens S, Vandenberghe S and Lemahieu I 2008 Acceleration of GATE SPECT simulations *Med. Phys.* **35** 1476–85

de Jong H W A M, Slijpen E T P and Beekman F J 2001 Acceleration of Monte Carlo SPECT simulation using convolution-based forced detection *IEEE Trans. Nucl. Sci.* **48** 58–64

Derenzo S E 1979 Precision measurements of annihilation point spread distributions for medically important positron emitters *Positron Annihilation* ed R R Hasiguti and K Fujiwara (Sendai: The Japan Institute of Metals) pp 819–23

Derenzo S E 1986 Mathematical removal of positron range blurring in high resolution tomography *IEEE Trans. Nucl. Sci.* **33** 565–69

Descourt P, Carlier T, Du Y, Song X, Bubat I, Frey E C, Bardies M, Tsui B M W and Visvikis D 2010 Implementation of angular response function modeling in SPECT simulations with GATE *Phys. Med. Biol.* **55** N253–66

de Wit T C, Xiao J, Nijsen J F W, van het Schip F V, Staelens S G, van Rijk P P and Beekman F J 2006 Hybrid scatter correction applied to quantitative holmium-166 SPECT *Phys. Med. Biol.* **51** 4773–87

Du Y, Frey C, Wang W T, Tocharoenchai C, Baird W H and Tsui B M W 2002 Combination of MCNP and SimSET for Monte Carlo simulation of SPECT with medium- and high-energy photons *IEEE Trans. Nucl. Sci.* **49** 668–74

Du Y, Tsui B M W and Frey E C 2006 Model-based compensation for quantitative $^{123}$I brain SPECT imaging *Phys. Med. Biol.* **51** 1269–82

Farncombe T H, Gifford H C, Narayanan M V, Pretorius H, Frey E C and King M A 2004 Assessment of scatter compensation strategies for $^{67}$Ga SPECT using numerical observers and human LROC studies *J. Nucl. Med.* **45** 802–12

Floyd C E, Jaszczak R J, Greer K L and Coleman R E 1986 Inverse Monte Carlo as a unified reconstruction algorithm for ECT *J. Nucl. Med.* **27** 1577–85

Funk T, Després P, Barber W C, Shah K S and Hasegawa B H 2006 A multipinhole small animal SPECT system with submillimeter spatial resolution *Med. Phys.* **33** 1259–68

Frey E C, Gilland K L and Tsui B M W 2002 Application of task-based measures of image quality to optimization and evaluation of three-dimensional reconstruction-based compensation methods in myocardial perfusion SPECT *IEEE Trans. Med. Imaging* **21** 1040–50

Frey E C and Tsui B M W 1994 Modeling the scatter response function in inhomogeneous scattering media for SPECT *IEEE Trans. Nucl. Sci.* **41** 1585–93

Gieles M, de Jong H W A M and Beekman F J 2002 Monte Carlo simulations of pinhole imaging accelerated by kernel-based forced detection *Phys. Med. Biol.* **47** 1853–67

Goorden M C and Beekman F J 2010a High-resolution tomography of positron emitters with clustered pinhole SPECT *Phys. Med. Biol.* **55** 1265–77

Goorden M C, van der Have F, Kreuger R and Beekman F J 2010b Sub-millimeter SPECT/PET with clustered pinholes: first experimental results *IEEE NSS/MIC Meeting Abstracts* pp M15-1

He B, Du Y, Song X, Segars W P and Frey E C 2005 A Monte Carlo and physical phantom evaluation of quantitative $^{111}$In SPECT *Phys. Med. Biol.* **50** 4169–85

Jan S *et al* 2004 GATE: a simulation toolkit for PET and SPECT *Phys. Med. Biol.* **49** 4543–61

Kadrmas D J, Frey E C and Tsui B M W 1998 Application of reconstruction-based scatter compensation to thallium-201 SPECT: implementations for reduced reconstructed image noise *IEEE Trans. Med. Imaging* **17** 325–33

Kamphuis C, Beekman F J, van Rijk P P and Viergever M A 1997 Dual matrix ordered subsets reconstruction for accelerated 3D scatter compensation in single-photon emission tomography *Eur. J. Nucl. Med.* **25** 8–18

Levin C S and Hoffman E J 1999 Calculation of positron range and its effect on the fundamental limit of positron emission tomography system spatial resolution *Phys. Med. Biol.* **44** 781–99

Liu S, King M A, Brill A B, Stabin M G and Farncombe T H 2008 Accelerated SPECT Monte Carlo simulation using multiple projection sampling and convolution-based forced detection *IEEE Trans. Nucl. Sci.* **55** 560–7

Meikle S R, Hutton B F and Bailey D L 1994 A transmission-dependent method for scatter correction in SPECT *J. Nucl. Med.* **35** 360–7

Meng L J, Rogers W L, Clinthorne N H and Fessler J A 2003 Feasibility study of compton scattering enhanced multiple pinhole imager for nuclear medicine *IEEE Trans. Nucl. Sci.* **50** 1609–17

Metzler S D, Bowsher J E, Greer K L and Jaszczak R J 2002 Analytic Determination of the pinhole collimator's point-spread function and RMS resolution with penetration *IEEE Trans. Med. Imaging* **21** 878–87

Moore S C, Ouyang J, Park M A and El Fahkri G 2006 Monte Carlo-based compensation for patient scater, detector scatter and crosstalk contamination in $^{111}$In SPECT imaging *Nucl. Instrum. Methods Phys. Res.* A **569** 472–6

Narayanan M V, Pretorius P H, Dahlberg S T, Leppo J A, Botkin N, Krasnow J, Berndt W, Frey E C and King M A 2003 Evaluation of scatter compensation strategies and their impact on human detection performance Tc-99m myocardial perfusion imaging *IEEE Trans. Nucl. Sci.* **50** 1522–7

Ruangma A, Bai B, Lewis J S, Sun X, Welch M J, Leahy R and Laforest R 2006 *Nucl. Med. Biol.* **33** 217–26

Santin G, Strul D, Lazaro D, Simon L, Krieguer M, Martins M V, Breton V and Morel C 2003 GATE: A Geant4-based simulation platform for PET and SPECT integrating movement and time management *IEEE Trans. Nucl. Sci.* **50** 1516–21

Schramm N U, Ebel G, Engeland U, Schurrat T, Béhé M and Behr T M 2003 High-resolution SPECT using multipinhole collimation *IEEE Trans. Nucl. Sci.* **50** 315–20

Shokouhi S, Metzler S D, Wilson D W and Peterson T E 2009 Multi-pinhole collimator design for small-object imaging with SiliSPECT: a high-resolution SPECT *Phys. Med. Biol.* **54** 207–25

Staelens S G, de Wit T C and Beekman F J 2007 Fast hybrid SPECT simulation including efficient septal penetration modelling (SP-PSF) *Phys. Med. Biol.* **52** 3027–43

Staelens S and Buvat I 2009 Monte Carlo simulations in nuclear medicine imaging *Advances in Biomedical Engineering* ed P Verdonck (Amsterdam: Elsevier) pp 177–209, chapter 5

Staelens S, Strul D, Santin G, Vandenberghe S, Koole M, d'Asseler Y, Lemahieu I and Van de Walle R 2003 Monte Carlo simulations of a scintillation camera using GATE: validation and application modelling *Phys. Med. Biol.* **48** 3021–42

Staelens S, Vunckx K, De Beenhouwer J, Beekman F J , D'Asseler Y, Nuyts J and Lemahieu I 2006 GATE simulations for optimization of pinhole imaging *Nucl. Instrum. Methods Phys. Res.* A **569** 359–63

Strul D, Santin G, Lazaro D, Breton V and Morel C 2003 GATE (Geant4 application for tomographic emission): a PET/SPECT general-purpose simulation platform *Nucl. Phys.* B **125** 75–9

Tai Y C, Wu H, Pal D and O'Sullivan J A 2008 Virtual-pinhole PET *J. Nucl. Med.* **49** 471–9

van der Have F, Vastenhouw B, Ramakers R M, Branderhorst W, Krah J O, Ji C, Staelens S G and Beekman F J 2009 U-SPECT-II: an ultra-high-resolution device for molecular small-animal imaging *J. Nucl. Med.* **50** 599–605

Vastenhouw B and Beekman F J 2007 Submillimeter total-body murine imaging with U-SPECT-I *J. Nucl. Med.* **48** 487–93

Vunckx K, Nuyts J, Vanbilloen B, De Saint-Hubert M, Vanderghinste D, Rattat D, Mottaghy F M and Defrise M 2009 Optimized multipinhole design for mouse imaging *IEEE Trans. Nucl. Sci.* **56** 2696–705

Walrand S H M, Elmbt L R and Pauwels S 1994 Quantitation in SPECT using an effective model of the scattering *Phys. Med. Biol.* **39** 719–34

Wang H, Jaszczak R J and Coleman R E 1992 Solid geometry-based object model for Monte Carlo simulated emission and transmission tomographic imaging systems *IEEE Trans. Med. Imaging* **11** 361–72

Xiao J, De Wit T C, Staelens S G and Beekman F J 2006 Evaluation of 3D Monte Carlo-based scatter correction for $^{99m}$Tc cardiac perfusion SPECT *J. Nucl. Med.* **47** 1662–9

Xiao J, De Wit T C, Zbijewski W, Staelens S G and Beekman F J 2007 Evaluation of 3D Monte Carlo-based scatter correction for $^{201}$Tl cardiac perfusion SPECT *J. Nucl. Med.* **48** 637–44

Zaidi H 1999 Relevance of accurate Monte Carlo modeling in nuclear medical imaging *Med. Phys.* **26** 574–608

Zubal G and Harrell C 1991 Voxel-based Monte Carlo calculations of nuclear medicine images and applied variance reduction techniques *Information Processing in Medical Imaging, Lecture Notes in Computer Science* vol 511 (Berlin: Springer) pp 23–33